ACS APPLIED MATERIALS & INTERFACES

RESEARCH ARTICLE

www.acsami.org

Parinaric Acid Methyl Ester Polymer Films with Hill-Structured Features: Fabrication and Different Sensitivities to Normal and Tumor Cells

Hua-Jie Wang,* Ying Cao, Cui Cao, Yuan-Yuan Sun, Xue-Hong Yu, Li-Fang Zhu, and Lin Yang*

College of Chemistry and Environmental Science, Henan Normal University, 46 East of Construction Road, Xinxiang 453007, People's Republic of China

ABSTRACT: Parinaric acid methyl ester (PnA-Me) polymer films with hill-structured features were fabricated by a solvent volatilization in situ cross-linking method. Moreover, nuclear magnetic resonance, Fourier transform infrared, and oxidation kinetic analyses were successfully applied to monitor the formation process of PnA-Me polymer films. The role of PnA-Me monomer concentrations for growth control of the hill structures on a glass matrix had also been investigated. Also, the results demonstrated that size control of the resulting hill structure ranging from 0.56 ± 0.18 to 19.6 ± 3.5 μm could be realized by varying the concentration of the PnA-Me monomer from 0.0117 to1.5 mg/mL. Additionally, the effects of polymer films with different surface topographical structures on the behaviors of rat mesenchymal stem cells and human pheochromocytoma cells were measured by morphological and metabolic methods. The results revealed that the cell activity of PnA-Me films was topographical structure- and cell-type-dependent. Furthermore, the selective sensitivity of the PnA-Me films to normal and tumor cells supported the potential value as the coatings for the tissue engineering substitutes.

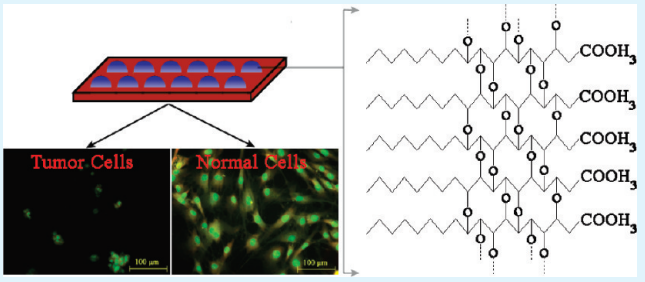

KEYWORDS: parinaric acid methyl ester, polymer film, topography, selective sensitivity, coatings, tissue engineering

1. INTRODUCTION

With the growth in incidence of tissue or organ implantation, there is a keen interest in the preparation of the bioactive substitutes for the reconstruction of diseased tissues in recent years. However, keeping in mind the significant lack of bioactivity for many substitutes, the coating technique is currently a focus of attention, linked to the improvement of biomaterials functions.[1−3] It is mainly due to the fact that the behaviors of the attachment, adhesion, spreading, and proliferation of the anchorage-dependent cells on materials rely heavily on the surface characteristics, such as chemistry, hydrophilicity/hydrophobicity, or surface free energy, charge, and rigidity.[4] As one of the typical surface characteristics, the physical structure of a biomaterial in both micrometer and nanometer scales has previously been demonstrated to be an important feature for controlling the responses of cells in vitro and vivo.[5−7] For example, Biela et al. fabricated the grooves with lateral dimensions of 2−10 μm and depths of 50−200 nm on poly(dimethylsiloxane) and investigated the sensitivity of human endothelial cells (ECs), smooth muscle cells (SMCs), and fibroblasts (FCs) to topographical signals.[8] They demonstrated that the orientation of all three cell types increased with smaller lateral spacing and with increasing depth of the grooves on the material surface, but FCs were much more sensitive to the topographical signals than ECs and SMCs. Up to now, it has been concluded that the surfaces with nano- or microtopographical structure can resemble the natural extracellular matrix, supply many more sites for protein adsorption, elicit specific cellular responses, and direct new tissue formation.[9−12] Consequently, considerable advances have already been made in attempts to designedly fabricate the coatings with the special topography.[13−16]

Recently, special attention has been given to parinaric acid (PnA) because of their four-conjugated polyunsaturated structure and their potential as fluorescent membrane probes in photophysical and biophysical studies, including the lipid−protein interactions, lipid clustering, lipid transport processes, characterization of lipoproteins, fatty acid binding proteins, and phospholipids transfer proteins.[17−21] However, PnA and its derivatives as the coating materials applied in medicine or life science have never been studied. In the present study, we reported a solvent volatilization−in situ cross-linking method to fabricate the PnA-Me polymer films with hill-structured features and size control of the hill-shaped structure was successfully realized. Here, rat mesenchymal stem cells (MSCs) and human pheochromocytoma cells (PC12) were chosen as the models of normal and tumor cells, respectively. The spread, proliferation, and metabolism of cells were examined by morphological and metabolic methods based on fluorescent microscopy observation, scanning electron microscopy (SEM) observation, and succinic dehydrogenase activity. The physicochemical

Received: May 2, 2011
Accepted: June 20, 2011
Published: June 20, 2011

and functional features support the potential value of the PnA-Me polymer films as coating materials applied in the tissue engineering field to adjust the different cell growth.

2. MATERIALS AND METHODS

2.1. Materials. Parinari glaberrimum seeds were obtained from a local seed company (Sanhe-Tian, Xinxiang, Henan, China). Seed oil was extracted in hexane and concentrated in a rotary evaporator at 30 °C (RE-52 rotary evaporator, Shanghai, China). Hexane was HPLC grade. All other solvents and chemicals were analytical grade.

2.2. Preparation of PnA and PnA-Me. *2.2.1. Preparation of PnA.* The seed oil was saponified in 300 mL of fresh 5% methanolic KOH under dinitrogen protection for 4 h at 65 °C. After acidification, free fatty acid at the top layer was collected and PnA was purified by repeated recrystallization from petroleum ether at −15 °C.

2.2.2. Methylation of PnA. PnA (20 mg) was methylated with 2 mL of 1.5 M H_2SO_4/methanol in 15 mL tubes with Teflon-lined screw caps. After being flushed with nitrogen gas and sealed tightly, the methylation tubes were placed in a heat block at 45 °C for 1 h. Then hexane (3 mL) and distilled water (1 mL) were added and mixed thoroughly. After centrifugation (4000 rpm/min), the top hexane layer containing PnA-Me was collected and stored at −20 °C.

2.3. Fabrication of Topographical Surfaces. The hill-structured surfaces were fabricated by the solvent volatilization−in situ cross-linking method. Briefly, the PnA-Me monomer was dissolved in ethanol with a final concentration of 0.0117−1.5 mg/mL. Then 40 μL of a PnA-Me monomer alcoholic solution was dropped onto the glass surface with a diameter of 9 mm and dried through volatilization at room temperature. After exposure to air for a given time interval at 37 °C, the samples were scratch out and dissolved in a chloroform solution. The oxidation kinetics of samples were analyzed by measuring the absorbance of PnA-Me at 302 nm using an UV−vis spectrophotometer (TU-11900, Beijing Purkinje General Instrument Co., Ltd., China). The typical PnA-Me polymer films were obtained after over 12 h of reaction at 37 °C.

2.4. Characteristics of the PnA-Me Polymer Films. *2.4.1. Nuclear Magnetic Resonance (NMR) Analysis.* All NMR experiments were recorded on a Bruker AV-400 Fourier transform NMR spectrometer (Bruker, Fallanden, Switzerland). Tetramethylsilane (TMS; 0.2−0.3 mM) in deuteriochloroform was used as an internal reference standard. Chemical shifts were given in δ values in ppm downfield from TMS ($\delta_{TMS} = 0$). ^{1}H and ^{13}C NMR spectrometry was conducted to assign the chemical shifts of the hydrogen and carbon atoms of the samples.

2.4.2. Fourier Transform Infrared (FTIR) Spectra. For FTIR analysis, the PnA-Me polymer film products on the glass were scraped off, mixed with KBr powder, and then pressed into pellets directly for FTIR determination on a Bio-Rad FTS-40 FTIR spectrograph in the wavenumber range of 4000−400 cm^{-1}. Also, the spectra were collected at 2 cm^{-1} resolution with 128 scans.

2.4.3. Morphology Observation. Surface morphologies of samples were observed by using a scanning electron microscope (JSM6390LV; JEOL, Tokyo, Japan) after being coated with gold in a vacuum. The size of the hill-shaped structure was randomly measured in each image with Image-Pro Discovery, version 4.5 (Media Cybernetics Inc.).

2.4.4. Aqueous Contact-Angle Analysis. The wettabilities of the samples were evaluated as static water contact angles using a contact-angle goniometer (OCA20; Data Physics, Bad Vilbil, Germany) according to our previous work.[22−24] Briefly, a droplet of water (3 μL, ultrapure grade) was put on the surfaces of the PnA-Me polymer films and the images were photographed, with the temperature and moisture content being kept constant during the course of the experiments (23 °C and 68%, respectively). The angle between the baseline of the drop and the tangent at the drop boundary was measured. Measurements were performed at least in triplicate on three different batches of material.

2.5. Responses of MSCs to PnA-Me Polymer Films. *2.5.1. MSC Culture.* Six-week-old female Sprague−Dawley rats with weights ranging from 215 to 237 g were sacrificed by ether. Rat femurs and tibiae were carefully cleaned of adherent soft tissue. The epiphyses were removed with a rongeur, and the marrow were flushed out by a syringe (21-gauge needle) with 4 mL of a low-glucose Dulbecco's Modified Eagle's complete medium (Eagle, Sigma, St. Louis, MO), supplemented with 20% fetal bovine serum, 100 units/mL penicillin, and 100 μg/mL streptomycin. This cell suspension was added slowly on the surface of a Percoll solution (1.073 g/mL) with a ratio of 3−5. Then centrifugation was perform at 2000 rpm for 20 min. Nucleated cells at the medium−Percoll interface were collected and then washed and plated in culture flasks at 5×10^4 cell/mL with a complete medium. The cells were incubated at 37 °C in a humidified 5% CO_2 environment, and the medium was changed every 3 days.

PC12 cells were routinely cultured in tissue culture flasks with a high-glucose Dulbecco's Modified Eagle's medium, containing 10% total bovine serum and incubated at 37 °C in a humidified atmosphere with 95% air and 5% CO_2. The culture medium was refreshed every 2 days.

2.5.2. Cell Seeding. When the cells became almost confluent, they were detached by treatment with 0.25% trypsin for 2−3 min at 37 °C. Before cell seeding, the PnA-Me polymer films were placed in a 48-well culture plate, sterilized by UV for 20 min, and then equilibrated with a prewarmed medium for 2 h. After removal of the medium from the wells by pipetting, the cells were counted to 10^4 cells/mL and 500 μL of the cell suspension was poured onto each substrate.

2.5.3. Cell Proliferation and Distribution. The cell distribution was observed by using the fluorescence microscope, and cell proliferation on the PnA-Me polymer films was measured by the cell counting method. Briefly, after 2 days of cell culture, all substrates were rinsed in phosphate-buffered saline (PBS; pH 7.2, 0.1 mol/L), and the cells attached to the surfaces were stained with acridine orange fluorescent dye in PBS for 5 min. Then the cells were counted on the fluorescence microscope (Axioskop 40; Carl Zeiss, Göttingen, Germany).[23−25]

2.5.4. Cell Viability. The metabolic analysis was performed by a 3-(4,5-dimethylthiazol-2-yl)-2,5-diphenyltetrazolium bromide assay (MTT) based on succinic dehydrogenase actthe ivity at OD 490 nm ($n = 3$); 630 nm was chosen as the reference wavelength. Briefly, after 2 days of cell culture, the wells were carefully washed with PBS. A total of 20 μL of MTT was added in 180 μL of a culture medium, and cell culture was continued for another 4 h. Then the solution was removed, and the wells were washed twice with PBS. A total of 200 μL of dimethyl sulfoxide was pipetted into the wells, and OD values were read on a microplate reader (Multiskan MK3; Thermo Labsystems, Hudson, NH).[26]

2.5.5. Cell Morphology Analysis. Cell spread on the substrate surfaces was observed by SEM. First, the samples were taken out randomly after 2 days of cell culture and washed with PBS. The cells were then fixed by immersing the samples into a 2.5% glutaraldehyde solution and allowing them to stand in the fixative at 4 °C for over 2 h. Then standard dehydration in an ethanol-graded series was performed. Finally, the samples were mounted on stubs, coated with gold in a vacuum, and examined by SEM.

2.6. Statistical Analysis. The number of independent replicas was listed individually for each experiment. Where applicable, all data were mean ± standard deviation (SD). Analysis of data was performed by one-way factorial analysis of variances (ANOVA) and multiple comparisons (Fisher's method as a post-hoc test, $p < 0.05$).

3. RESULTS

In order to present the data clearly, PnA-Me polymer films with different hill-shaped structures were abbreviated as

PnA-Me[1], PnA-Me[1/2], PnA-Me[1/8], PnA-Me[1/16], and PnA-Me[1/128], respectively, according to the ratio of the corresponding monomer concentration in the film processing to 1.5 mg/mL.

3.1. Characteristics of PnA-Me Polymer Films. PnA-Me polymer films were fabricated by the solvent volatilization—in situ cross-linking method. In order to find a suitable reaction period, the oxidative kinetics of the PnA-Me monomer on a glass matrix in air at 37 °C were first analyzed. As shown in Figure 1, the PnA-Me monomer is unstable, with 31.3% of the monomer being lost after exposure to air for 60 min. A total of 270 min later, the percentage of the oxidized PnA-Me monomer reaches 98.7%. Therefore, the typical PnA-Me polymer films were obtained after over 12 h of reaction at 37 °C.

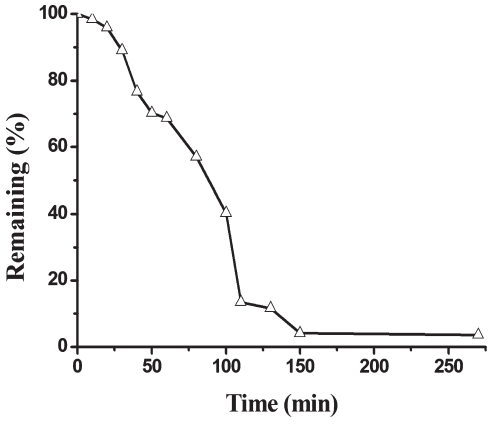

Figure 1. Stability of PnA-Me solid films on a glass matrix at 37 °C.

To further identify the structure of PnA-Me polymer films, the samples before and after polymerization were characterized by NMR and FTIR spectra, respectively. Figure 2 shows the ^{1}H and ^{13}C NMR spectra of the PnA-Me monomer and the PnA-Me polymer. It can be seen that the PnA-Me monomer shows signals at δ_H 5−7 ppm and δ_C 125−140 ppm, which correspond to the shifts of olefinic protons and carbons (Figure 2A$_1$,B$_1$). As for the PnA-Me polymer, the ^{1}H and ^{13}C NMR spectra are shown in Figure 1B$_1$,B$_2$. By comparison with Figure 2A$_1$, it is clear that the signals of olefinic protons of the PnA-Me monomer disappear in Figure 2A$_2$. Meanwhile, signals at δ_H 1.5−2 ppm enhance significantly, which can be assigned as the chemical shifts of alicyclic protons. In addition, new signals at δ_H 3−4 ppm appear, which can be assigned as the chemical shifts of protons in a peroxide bridge. All of these changes clearly show that the

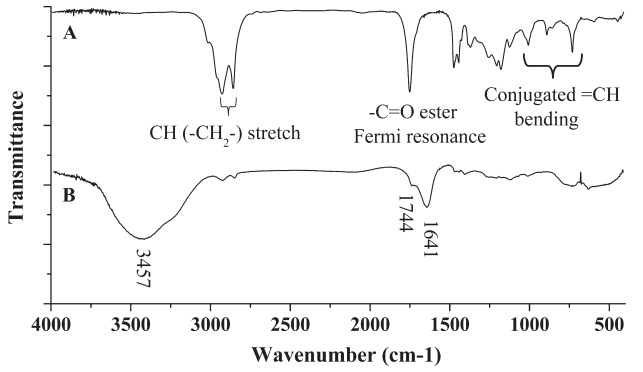

Figure 3. FTIR spectra of the PnA-Me monomer (A) and PnA-Me polymer films (B).

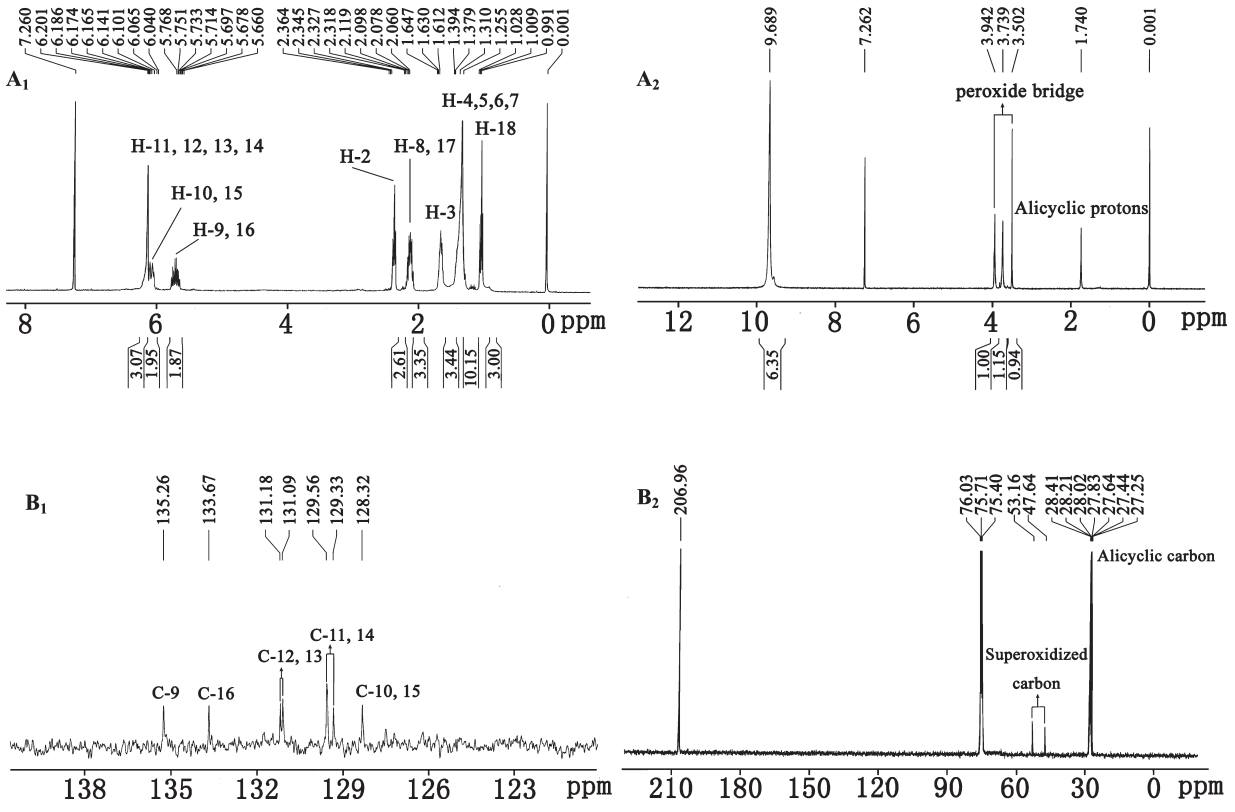

Figure 2. H[1] NMR (A) and C[13] NMR (B) spectra of the PnA-Me monomer (1) and PnA-Me polymer films (2).

Table 1. Some of the IR Band Assignments of PnA-Me before and after Polymerization

frequency (cm^{-1})	functional group and mode of vibration
3457	−OH stretching
2934, 2857	CH (−CH_2−) stretching
1744	−C═O ester Fermi resonance
1641	−C═C− stretching
1467	−CH (−CH_2−, CH_3) bending
1362	−CH (CH_3) symmetric bending
1247, 1171	−CO, −CH_2− stretching, bending
1116	−CO stretching
670−1050	conjugated ═CH bending

PnA-Me monomer transforms into the PnA-Me polymer through a peroxidization and cyclization process. Similarly, the superoxidized and alicyclic signals can be observed in the ^{13}C NMR spectrum of the PnA-Me polymer, as shown in Figure $2B_2$. Both the disappearance of olefinic carbon signals and the enhancement of alicyclic carbon signals at δ_C 23−28 ppm can further confirm the alicyclic structure in the PnA-Me polymer (Figure $2B_1$,B_2). Besides, the appearance of signals at δ_C 45−55 ppm also reveals the existence of a superoxidized structure.

Figure 3 shows the FTIR spectra of the PnA-Me polymer film before and after polymerization, and the corresponding IR adsorptions arising from the functional groups in samples are shown in Table 1. Before polymerization, the PnA-Me monomer shows the characteristic peaks of ester at about 1744 cm^{-1}. The typical absorption peaks of conjugated double bonds appear at

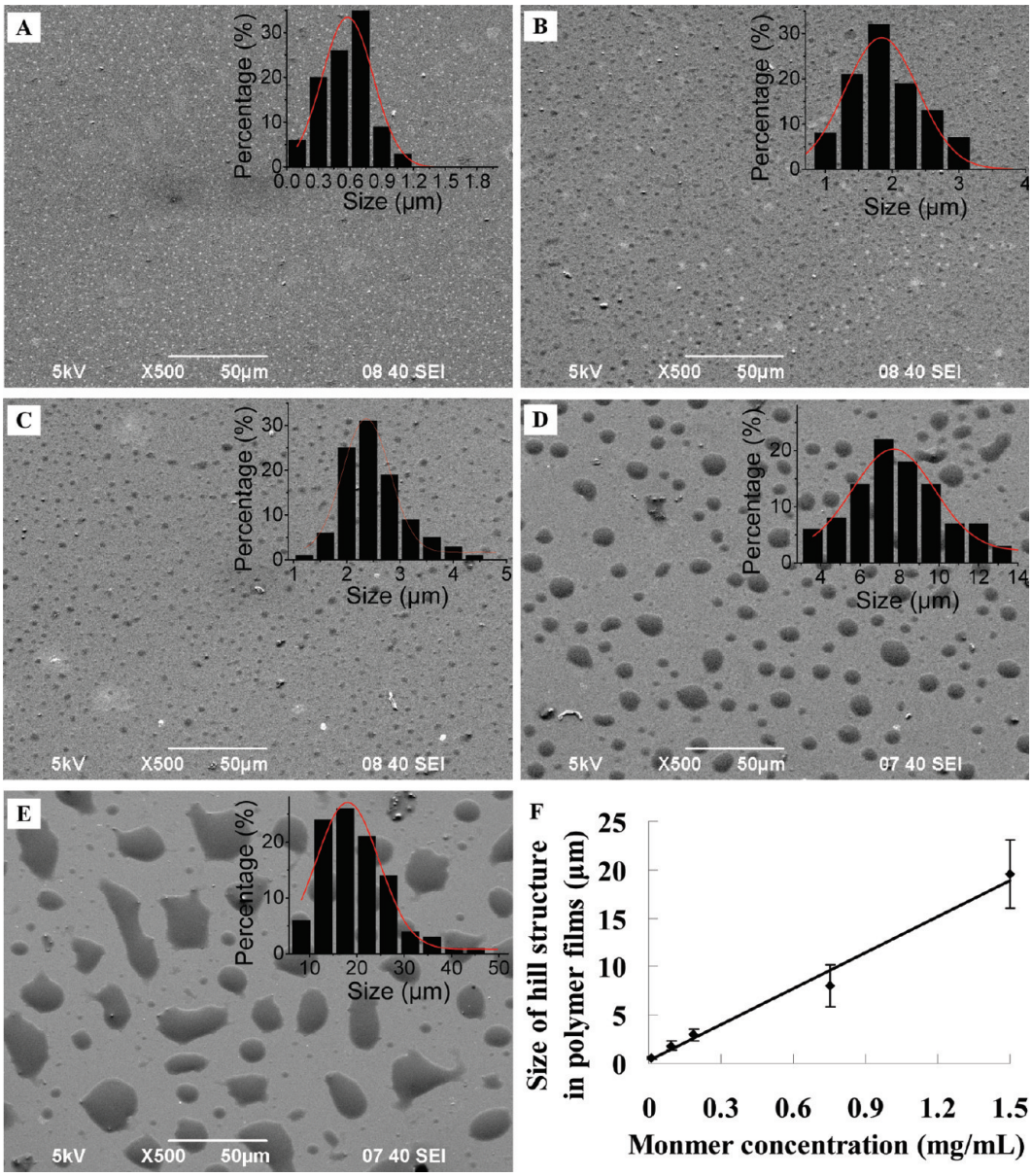

Figure 4. SEM images of the PNA-Me polymer films on a glass matrix prepared by the solvent volatilization−in situ cross-linking method with different concentrations of the PNA-Me monomer: (A) 0.0117 mg/mL; (B) 0.0938 mg/mL; (C) 0.1875 mg/mL; (D) 0.75 mg/mL; (E) 1.5 mg/mL; (F) the linearity curve of the PNA-Me concentrations and the diameters of the hill-shaped patterns.

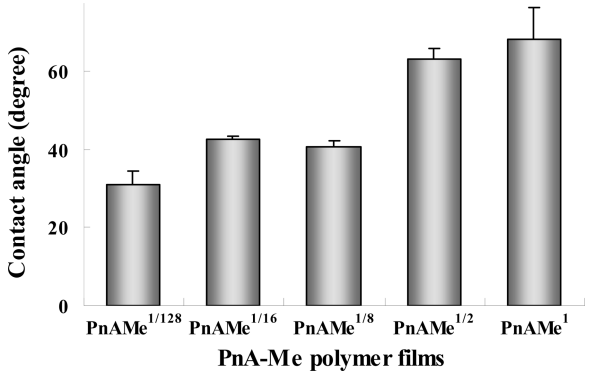

Figure 5. Aqueous contact angles of the PNA-Me polymer films on a glass matrix prepared by the solvent volatilization−in situ cross-linking method with different concentrations of the PNA-Me monomer.

999, 881, and 721 cm^{-1}, respectively. In addition, the spectra in the range of 3400−3600 cm^{-1} show no peroxide peak and indicate no significant oxidation in the PnA-Me monomer (Figure 3A). After exposure to air for 12 h at 37 °C, the consequent generation of free hydroxyl groups results in a typical peroxide peak at 3457 cm^{-1}, indicating significant oxidation in the PnA-Me polymer films. Moreover, the disappearance of conjugated double bonds in the range of 670−1050 cm^{-1} and the appearance of a double-bond stretching peak at 1641 cm^{-1} demonstrate that the cross-linking reaction in the polymer films occurs (Figure 3B).

The morphologies of the PnA-Me polymer films were observed by SEM, and the images are shown in Figure 4. All of the polymer films are composed of the hill-shaped pattern with different sizes corresponding to the different PnA-Me monomer concentrations and keep well-dispersity on the film surfaces (Figure 4A−E). The insets in Figure 4A−E show the corresponding size distribution of the hill-shaped pattern. It can be seen that, although the hill-shaped pattern in each film is inhomogeneous, the mean diameter increases from 0.56 ± 0.18 to 19.6 ± 3.5 μm with an increase of the PnA-Me monomer concentration. Moreover, it keeps the well-linear relationship, and the correlation coefficient reaches 99.3% (Figure 4F).

The topographical change of the surfaces always results in a corresponding change in wettability and the water contact angles of PnA-Me polymer films were measured, as shown in Figure 5. With a decrease of the PnA-Me monomer concentration and the diameter of the hill-shaped pattern, the PnA-Me polymer films are more hydrophilic. They show 67.9 ± 8.2°, 63.0 ± 2.6°, 40.7 ± 1.6°, 42.4 ± 1.0°, and 30.9 ± 3.5°of water contact angles, respectively.

3.2. Cell Sensitivity to PnA-Me Surfaces with Different Topographies. Figure 6A shows the inhibition rate of PnA-Me polymer films with different topographical structures on MSCs measured by the metabolic method after 2 days of cell culture. It can be seen that cell viabilities for different topographical surfaces are significantly different on the basis of the succinic dehydrogenase activity analysis ($p < 0.05$, $n = 3$). There is a significant enhancement of the inhibition effects for both PnA-$Me^{1/2}$ and PnA-Me^{1} polymer films compared with PnA-$Me^{1/128}$, PnA-$Me^{1/16}$, and PnA-$Me^{1/8}$ polymer films, but no statistical difference is observed between PnA-$Me^{1/16}$ and PnA-$Me^{1/8}$ or between PnA-$Me^{1/2}$ and PnA-Me^{1}. Figure 6B shows the inhibition rate of PnA-Me polymer films on PC12 cells. Similarly, the metabolic

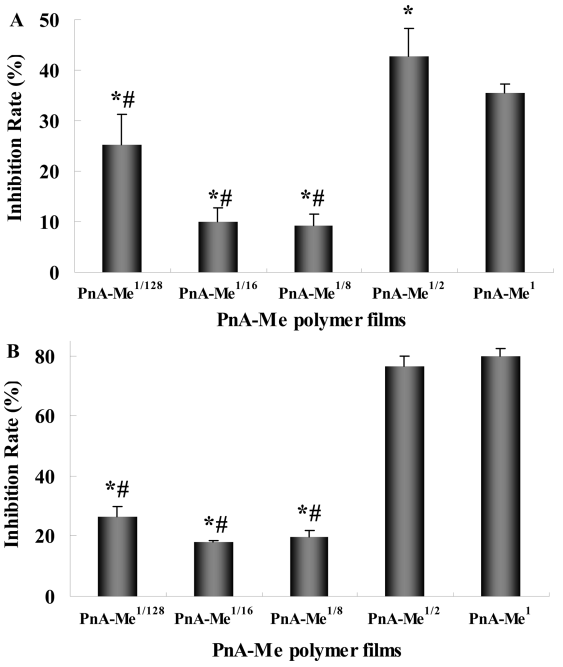

Figure 6. Proliferation of MSCs (A) and PC12 cells (B) on PNA-Me polymer films with different topographical structures determined by the MTT method based on the succinic dehydrogenase activity. Cells were seeded at 10^4 cells/mL and allowed to proliferate for 2 days. The data were expressed as mean ± SD ($n = 3$). Asterisks mean significant differences compared with the PnA-$Me^{1/128}$ group, and number signs mean significant differences compared with both PnA-Me^{1} and PnA-$Me^{1/2}$.

activity of PC12 cells on polymer films is also topographical structure-dependent. However, the PC12 cells indicate different sensitivities compared with MSCs, and the inhibition effects of PnA-Me on PC12 cells reached 1.0−2.5 times higher than those on MSCs.

In order to visualize cell morphologies on different PnA-Me polymer films, cells were stained using acridine orange and observed with a fluorescence microscope. Figure 7 shows a series of sequential images of MSCs and PC12 cells adhered onto the PnA-Me polymer films. MSCs distribute uniformly on the films and an almost confluent monolayer is observed on PnA-$Me^{1/8}$ and PnA-$Me^{1/16}$ polymer films (Figure $7B_1$,C_1). The numbers of adhered MSCs show a minimum on PnA-Me^{1} and PnA-$Me^{1/2}$ polymer films (Figure $7A_1$−E_1). The results obtained by the cell counting method are in agreement with those by the metabolic method. The cell densities are higher on the surfaces composed of the hill-shaped pattern with relatively smaller diameters, especially for PnA-$Me^{1/8}$, which is more favorable to MSC growth than other groups (Figure $7F_1$). Although PC12 cells on PnA-Me polymer films also indicate a similar trend for the cell density to MSCs, the cell morphologies and distributions were abnormal (Figure $7A_2$−E_2). PC12 cells aggregate, and most of them are round-shaped. These results indicate that PnA-Me polymer films are unfavorable to PC12 cell growth. Especially on PnA-Me^{1} and PnA-$Me^{1/2}$ polymer films, almost no cells are observed.

The spread of MSCs was observed by SEM, as shown in Figure 8. MSCs cultured on PnA-Me polymer films exhibit a flatter or irregular morphology with sizes of 50−80 μm and cover the film surfaces. Although the spread of MSCs on each polymer

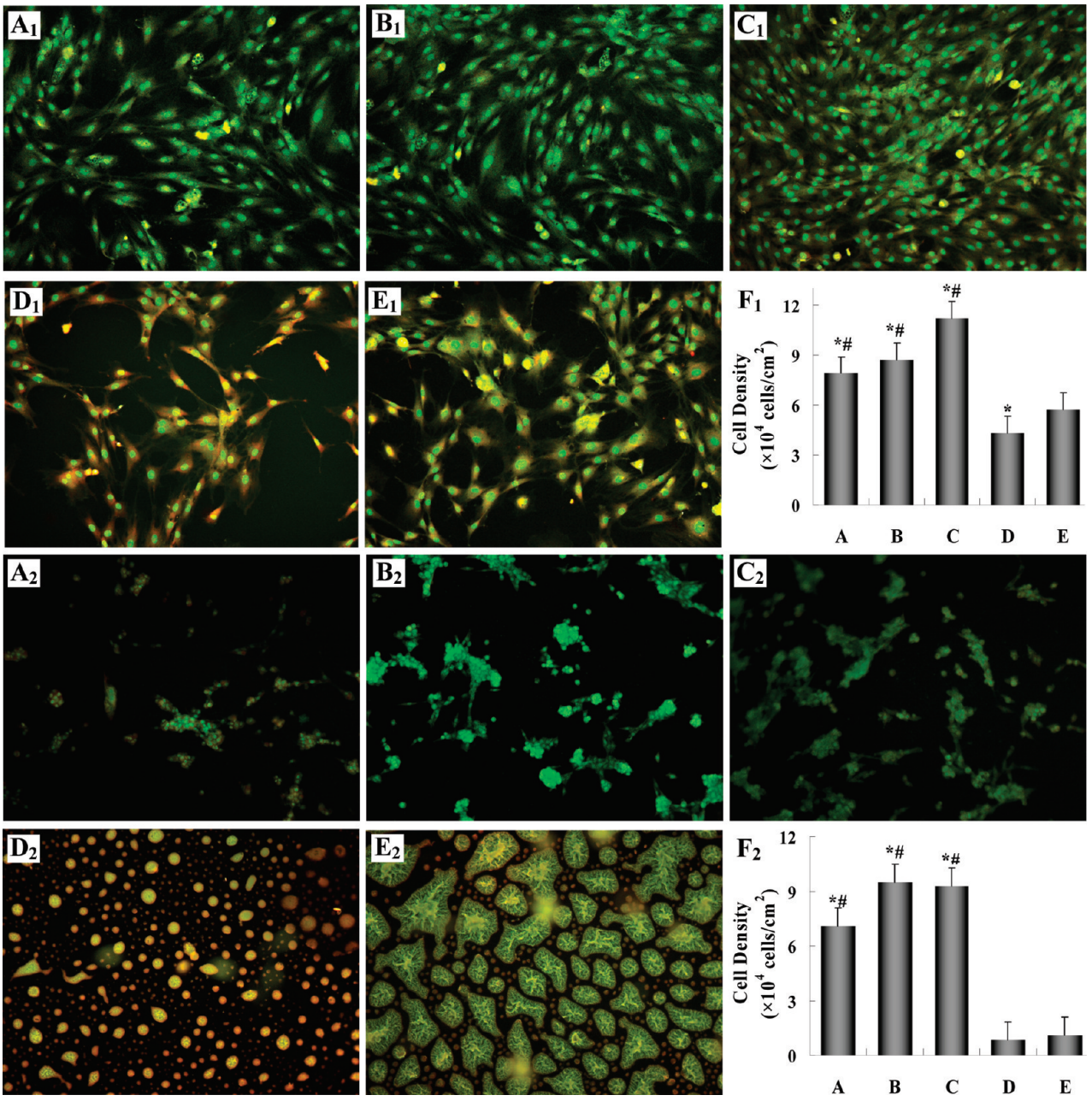

Figure 7. Morphologies and distributions of MSCs (1) and PC12 cells (2) on different PnA-Me polymer films after 2 days of cell culture observed by a fluorescent microscope (10× magnification): (A) PnA-Me$^{1/128}$; (B) PnA-Me$^{1/16}$; (C) PnA-Me$^{1/8}$; (D) PnA-Me$^{1/2}$; (E) PnA-Me^{1}. The corresponding cell densities of MSCs on different films determined by the cell counting method (F).

film has no significant difference based on the contact area analysis of cells (data not shown), the pseudopodium of cells on PnA-Me$^{1/8}$, PnA-Me$^{1/16}$, and PnA-Me$^{1/128}$ polymer films was more abundant than that on both PnA-Me^{1} and PnA-Me$^{1/2}$ polymer films. These results indicated that the PnA-Me polymer films composed of spherical particles with the smaller sizes were much better for MSC adhesion and spreading.

4. DISCUSSION

Tissue engineering is not a new concept, but there are many fundamental problems waiting to be solved to bring tissue engineering technology to clinical fruition. One of the major thrusts is to improve the biocompatibility of implants. Surface coatings had been demonstrated to be a useful method to improve the biocompatibility of tissue engineering materials.[27−29] As one of surface physical characteristics, the surface topographical structure is one of the important factors for biomaterials affecting or controlling the cellular behaviors or tissue responses.[30−33] In the present study, we prepared the PnA-Me polymer films with different topographical surfaces by the solvent volatilization−in situ cross-linking method based on the surface tension difference of the PnA-Me monomer and a glass, as the described in Scheme 1. The PnA-Me monomer has a high surface tension because of its high nonpolarity. Likewise, a glass has a hydroxyl group enriched surface and, consequently, causes a high polarity,

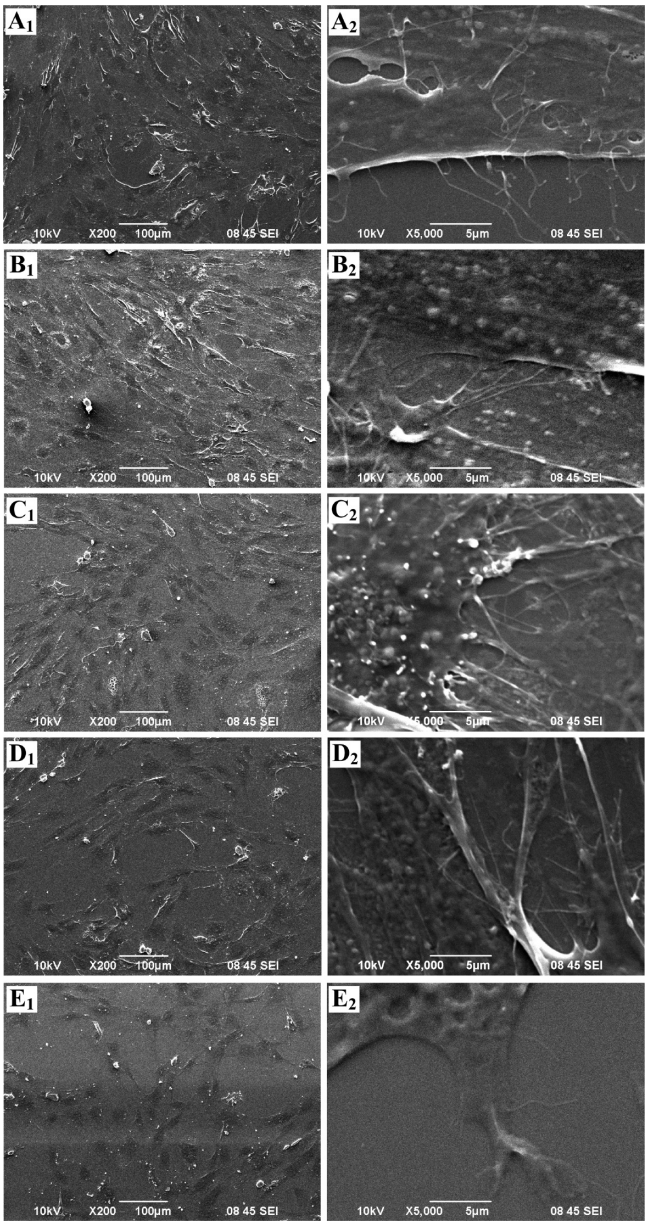

Figure 8. SEM images of MSCs on different PnA-Me polymer films after 2 days of cell culture: (A) PnA-Me$^{1/128}$; (B) PnA-Me$^{1/16}$; (C) PnA-Me$^{1/8}$; (D) PnA-Me$^{1/2}$; (E) PnA-Me^{1}.

which also results in a high surface tension. When the PnA-Me monomer was dropped onto the glass surface, the PnA-Me monomer would contract because of the tendency of the surface to want to form the smallest possible surface area. Therefore, the hill-shaped pattern, like a lens, would be its favorite structure. Moreover, the diameter of the hill-shaped pattern depended on the PnA-Me monomer concentration on the glass when the surface area was constant. After that, the PnA-Me hill-shaped pattern was allowed to in situ cross-link based on its conjugated double bonds.[34,35] Briefly, when PnA-Me was exposed to air, the direct attack on the double bonds by oxygen formed cyclic peroxides. The peroxides were needed because the polymerization catalysts and the resultant reaction of the peroxides with allylic methylene groups led to the formation of radicals. This created a radical chain reaction and finally formed the PnA-Me

Scheme 1. Possible Formation Pathway of PnA-Me Polymer Films Prepared by the Solvent Volatilization−in-Situ Cross-Linking Method

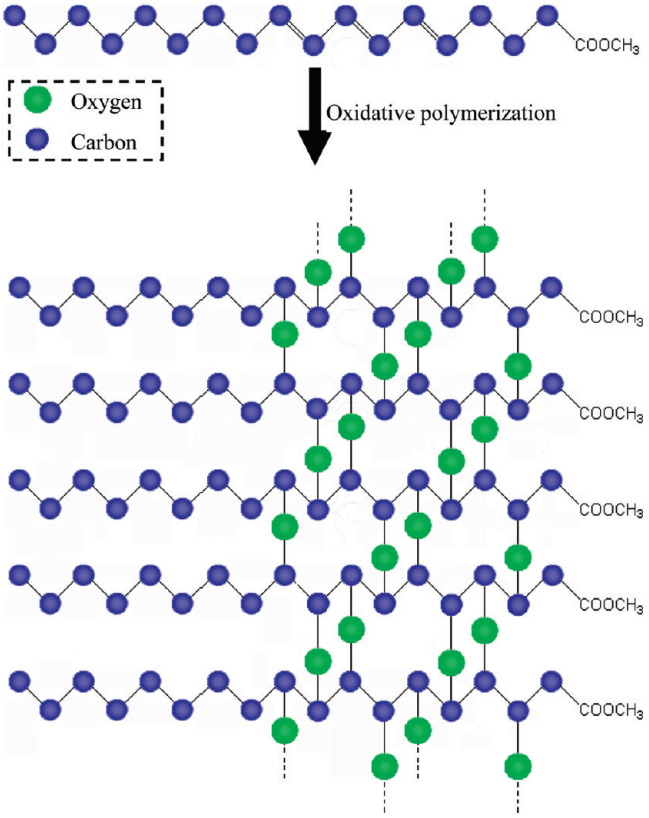

polymer films.[34,35] NMR and FTIR analysis (Figures 2 and 3 and Table 1) could demonstrate transformation from the PnA-Me monomer to the PnA-Me polymer. Followed by polymerization, the hill-shaped pattern of the PnA-Me polymer films on a glass could be stabilized (Figure 4). Taken together, the polarity of the matrix would greatly affect the size of the hill-shaped pattern. Besides, the size control could be realized by adjusting the PnA-Me monomer concentration. However, the interhill distance and hill height are irregular and are difficult to control in this work, as shown in Figure 4. Therefore, the size of the hill-shaped pattern was chosen as one of the typical parameters of topography to study the effects of the topographical structure on cell growth.

In order to clarify the influence of surfaces and assess the cell compatibility of the resulting polymer films, in vitro experiments were carried out to test the behavior of MSCs and PC12 cells, such as spread, proliferation, and metabolism on the PnA-Me polymer films. Both the metabolic and cell counting methods indicated that the metabolism and proliferation of MSCs and PC12 cells could be slightly inhibited by PnA-Me$^{1/8}$ and PnA-Me$^{1/16}$ polymer films, which were composed of 2.96 ± 0.19 and 1.83 ± 0.09 μm of the hill-shaped patterns, respectively. However, the inhibition of PnA-Me^{1} and PnA-Me$^{1/2}$ polymer films was significantly enhanced (Figure 6−8), which were composed of 8.0 ± 0.75 and 19.6 ± 1.5 μm of the hill-shaped patterns. It has been well documented that cell behaviors are influenced by the surface roughness and topographical structure.[6] For example, Green et al. found that nodes of 2 and 5 μm resulted in increased cell proliferation compared to 10 μm nodes and smooth

surfaces.[36] Biela et al. found that cells were more aligned along the grooves for the case of 2 μm spacing than 10 μm spacing.[8] In this study, all of the PnA-Me polymer films had the same chemical structure, but they were composed of hill-shaped patterns with different diameters. Therefore, the topographical difference among the PnA-Me polymer films might be the most important reason for affecting the metabolism and proliferation of MSCs and PC12 cells on them. In addition, a topographical change of the surfaces always results in a hydrophilic/hydrophobic change. For example, Chvedov and Arnold studied the relationship between the surface topography parameters and the contact angle of a aluminum sheet with different topographies, and they found that the contact angle was proportional to the lubricant-filled profile valley area (one of the surface topography parameters), with a slope related to the surface tension of the test liquid.[37] This relativity between the topographical structure and the contact angle was also verified in this study. The contact angle of the PnA-Me polymer films increased with an increase of their roughness and varied from 30.9 ± 3.5° to 67.9 ± 8.2°. Therefore, the wettability of a surface is needed to be considered for studies on the interaction of cells and the material surface. Arima and Iwata demonstrated that the number of adhered human umbilical vein ECs reached a maximum on CH_3/OH mixed self-assembled monolayers (SAMs) with a water contact angle of 40°, while cell adhesion increased with decreasing water contact angle up to 60−70° and then leveled off on CH_3/COOH and CH_3/NH_2 mixed SAMs. Moreover, the numbers of adhered HeLa cells showed a maximum on CH_3/OH and CH_3/COOH mixed SAMs. They considered that both surface wettability and cell types could affect cell adhesion.[38] The PnA-$Me^{1/8}$ and PnA-$Me^{1/16}$ polymer films had 42.4 ± 1.0° and 40.7 ± 1.6° of water contact angles, which were significantly different from that of PnA-Me^{1} (63.0 ± 2.6°), PnA-$Me^{1/2}$ (67.9 ± 8.2°), and PnA-$Me^{1/128}$ (30.9 ± 3.5°) polymer films. So, we considered that the approximately 40° of water contact angles of PnA-Me polymer films might be suitable for the growth of MSCs and PC12 cells.

Besides the physical properties of PnA-Me polymer films in this study affecting the cell behaviors, the cell type was also another worthy factor to be considered.[39] For example, Traynelis et al. reported that low concentrations of PnA destroyed rat and human malignant glioma cell lines and spared the normal rat astrocytes in culture. Moreover, their studies also demonstrated that a selective activation of c-Jun N-terminal protein kinase (JNK) and the opposite regulation of forkhead transcription factor-3a (FOXO3a) and mitochondrial superoxide dismutase (Mn-SOD) contributed to the differential cytotoxicity of PnA in malignant and normal glial cells.[19,20,40] In the present study, PnA-Me polymer films also showed the different inhibition effects on normal cells (MSCs) and tumor cells (PC12 cells). This selective inhibition effect of PnA-Me polymer films might exhibit its potential at the occurrence of the implant-associated tumor.[41] Therefore, our future efforts will focus on the detailed mechanism of this selective inhibition effect.

5. CONCLUSION

In summary, the PnA-Me polymer films composed of hill-shaped patterns with the different diameters ranging from 0.56 ± 0.18 to 19.6 ± 3.5 μm could be successfully fabricated by a solvent volatilization−in situ cross-linking method based on the surface tension difference of the PnA-Me monomer and a glass. The final diameters of the hill-shaped patterns depended on the concentration of the applied PnA-Me monomer. The change of the topographical structures of the PnA-Me polymer films would result in a change of the water contact angles from 30.9 ± 3.5° to 67.9 ± 8.2°. PnA-Me polymer films exhibited the topographical structure- and cell-type-dependent inhibition effects on cell metabolism, proliferation, and spread, which support the potential value of the PnA-Me polymer films as coating materials applied in the tissue engineering field.

AUTHOR INFORMATION

Corresponding Author

*Phone: +86-373-3325999. Fax: +86-373-3328507. E-mail: wanghuajie972001@163.com (H.-J.W.), yanglin1819@163.com (L.Y.).

ACKNOWLEDGMENT

This work was financially supported by the National Science Foundation of China (Grants 20971039 and 31000774), the National Key Basic Research and Development Program of China (Grant 2009CB626610), the Innovation Scientists and Technicians Troop Construction Projects of Henna Province (Grant 114200510004), and the National College Students Innovation Experiment Program (Grant 2009039).

REFERENCES

(1) Fernandez, I. C. S.; Busscher, H. J.; Metzger, S. W.; Grainger, D. W.; van der Mei, H. C. *Biomaterials* **2011**, *32*, 979–984.
(2) Suzuki, T.; Kubo, K.; Hori, N.; Yamada, M.; Kojima, N.; Sugita, Y.; Maeda, H.; Ogawa, T. *Biomaterials* **2010**, *31*, 4818–4828.
(3) Dong, Y.; Li, P.; Chen, C.-B.; Wang, Z.-H.; Wang, P.; Chen, G.-Q. *Biomaterials* **2010**, *31*, 8921–8930.
(4) Lee, S. J.; Khang, G.; Lee, Y. M.; Lee, H. B. *J. Colloid Interface Sci.* **2003**, *259*, 228–235.
(5) Riedel, M.; Müller, B.; Wintermantel, E. *Biomaterials* **2001**, *22*, 2307–2316.
(6) Miller, D. C.; Thapa, A.; Haberstroh, K. M.; Webster, T. J. *Biomaterials* **2004**, *25*, 53–61.
(7) Katsikogianni, M.; Missirlis, Y. F. *Eur. Cell Mater.* **2004**, *8*, 37–57.
(8) Biela, S. A.; Su, Y.; Spatz, J. P.; Kemkemer, R. *Acta Biomater.* **2009**, *5*, 2460–2466.
(9) Lee, J. H.; Lee, S. J.; Khang, G.; Lee, H. B. *J. Colloid Interface Sci.* **2000**, *230*, 84–90.
(10) Lee, J. W.; Lee, K. S.; Cho, N.; Ju, B. K.; Lee, K. B.; Lee, S. H. *Sens. Actuators, B* **2007**, *128*, 252–257.
(11) Arima, Y.; Iwata, H. *Biomaterials* **2007**, *28* (20), 3074–3082.
(12) Bakeine, G. J.; Ban, J.; Grenci, G.; Pozzato, A.; Zilio, S. D. *Microelectron. Eng.* **2009**, *86*, 1435–1438.
(13) Helary, G.; Noirclere, F.; Mayingi, J.; Migonney, V. *Acta Biomater.* **2009**, *5* (1), 124–133.
(14) Anselme, K.; Davidson, P.; Popa, A. M.; Giazzon, M.; Liley, M.; Ploux, L. *Acta Biomater.* **2010**, *6*, 3824–3846.
(15) Rosales-Leal, J. I.; Rodriguez-Valverde, M. A.; Mazzaglia, G.; Ramon-Torregrosa, P. J.; Diaz-Rodriguez, L.; Garcia-Martinez, O.; Vallecillo-Capilla, M.; Ruiz, C.; Cabrerizo-Vilchez, M. A. *Colloid Surf., A* **2010**, *365*, 222–229.
(16) Thapa, A.; Miller, D. C.; Webster, T. J.; Haberstroh, K. M. *Biomaterials* **2003**, *24*, 2915–2926.
(17) Zsila, F.; Bikadi, Z. *Spectrochim. Acta, Part A* **2005**, *62*, 666–672.
(18) Lopes, S.; Fernandes, M. X.; Prieto, M.; Castanho, M. A. R. B. *J. Phys. Chem. B* **2001**, *105*, 562–568.
(19) Zaheer, A.; Sahu, S. K.; Ryken, T. C.; Traynelis, V. C. *Neurochem. Res.* **2007**, *32*, 115–124.

(20) Traynelis, V. C.; Zaheer, A.; Sahu, S. K. *Int. Congr. Ser.* **2002**, *1247*, 297–309.
(21) Kuklev, D. V.; Smith, W. L. *Chem. Phys. Lipids* **2004**, *131*, 215–222.
(22) Wang, H. J.; Liu, X. M.; Ji, L. W.; Ma, D. L.; Ren, Q.; Wang, J. Y. *J. Biomed. Mater. Res., Part B* **2006**, *79B*, 411–419.
(23) Wang, H. J.; Ji, L. W.; Li, D. F.; Wang, J. Y. *J. Phys. Chem. B* **2008**, *112*, 2671–2677.
(24) Li, D. F.; Wang, H. J.; Fu, J. X.; Wang, W.; Jia, X. S.; Wang, J. Y. *J. Phys. Chem. B* **2008**, *112*, 16290–16299.
(25) Lovelace, M. D.; Cahill, D. M. *J. Neurosci. Methods* **2007**, *165*, 223–229.
(26) Alley, M. C. *Cancer Res.* **1998**, *48* (3), 589–601.
(27) Wang, H.; Fang, Y. E.; Yang, Y. *J. Mater. Chem.* **2001**, *11*, 1374–1377.
(28) Morimoto, N.; Watanabe, A.; Iwasaki, Y.; Akiyoshi, K.; Ishihara, K. *Biomaterials* **2004**, *25* (23), 5353–5361.
(29) Erli, H. J.; Ruger, M.; Ragoss, C.; Jahnen-Dechent, W.; Hollander, D. A.; Paar, O.; von Walter, M. *Biomaterials* **2006**, *27* (8), 1270–1276.
(30) Martinez, E.; Engel, E.; Planell, J. A.; Samitier, J. *Ann. Anat.* **2009**, *191*, 126–135.
(31) Flemming, R. G.; Murphy, C. J.; Abrams, G. A.; Goodman, S. L.; Nealey, P. F. *Biomaterials* **1999**, *20*, 573–588.
(32) Brunette, D. M.; Hamilton, D. W.; Chehroudi, B.; Waterfield, J. D. *Int. Congr. Ser.* **2005**, *1284*, 229–238.
(33) Liu, X. M.; Lim, J. Y.; Donahue, H. J.; Dhurjati, R.; Mastro, A. M.; Vogler, E. A. *Biomaterials* **2007**, *28*, 4535–4550.
(34) Lundberg, W. O. *J. Am. Oil Chem. Soc.* **1955**, *32*, 207–208.
(35) Hirota, S.; Itoh, U.; Sugi, M. *Thin Solid Films* **1985**, *134*, 67–74.
(36) Green, A. M.; Jansen, J. A.; ven der Waerden, J. P. C. M.; von Recum, A. F. *J. Biomed. Mater. Res.* **1994**, *28*, 647–653.
(37) Chvedov, D.; Arnold, A. *Ind. Eng. Chem. Res.* **2004**, *43*, 1541–1459.
(38) Arima, Y.; Iwata, H. *Biomaterials* **2007**, *28* (20), 3074–3082.
(39) Cornelius, A. S.; Yerram, N. R.; Kratz, D. A.; Spector, A. A. *Cancer Res.* **1991**, *51*, 6025–6030.
(40) Traynelis, V. C.; Ryken, T. C.; Cornelius, A. S. *Neurosurgery* **1995**, *37*, 484–489.
(41) Kirkpatrick, C. J.; Alves, A.; Kohler, H.; Kriegsmann, J.; Bittinger, F.; Otto, M.; Williams, D. F.; Eloy, R. *Am. J. Pathol.* **2000**, *156* (4), 1455–1467.